Non-linear constraints with application to self-potential source inversion

Burke J. Minsley, Jonathan Ajo-Franklin, and Frank Dale Morgan
Earth Resources Laboratory
Department of Earth, Atmospheric, and Planetary Sciences
Massachusetts Institute of Technology

May 2006

Abstract

We investigate the use of non-linear constraints for geophysical inverse problems, with specific examples applied to source inversion of self-potential data. Typical regularization methods often produce smooth solutions by introducing a quadratic term in the objective function that minimizes the L_2 norm of a low-order differential operator applied to the model. In some cases, however, the properties of interest may not vary smoothly. Two alternative constraints are examined that provide inversion stability while allowing for solutions with non-smooth properties. One method, often referred to as 'compactness' or 'minimum support', seeks to minimize the area (in 2D) or volume (in 3D) occupied by non-zero model parameters. The second method, 'total variation', minimizes an approximation of the L_1 norm of the gradient of the model. Both approaches involve a non-linear regularization functional, and must therefore be solved iteratively. We discuss the practical aspects of implementing these regularization methods and compare several examples using self-potential source inversion on a synthetic model. We also apply the compactness constraint for self-potential source inversion using a field data example.

1 Introduction

Most geophysical inverse problems are ill-posed and non-unique, and therefore require some form of regularization to ensure a stable solution. A common form of regularization involves the measure of a low order differential operator applied to the model [e.g. *Tikhonov and Arsenin*, 1977]. Minimization of this functional using an L_2 norm results in a linear system of equations that introduces stability through the constraints provided by the regularization operator. When the operator is the identity matrix (0^{th} order), a minimum length solution is obtained. Other popular operator choices include the gradient or Laplacian (1^{st} or 2^{nd} order), which produce flat or smooth solutions, respectively. *A-priori* information can be included, for example, by introducing anisotropic weights for the gradient operator to promote features such as horizontal layering. *Li and Oldenburg* [1996; 2000] employ a combination of metrics that enforce a minimum length solution with respect to a reference model, allow for anisotropic spatial gradients, and incorporate depth weighting to overcome problems related to poor sensitivity at depth.

These methods are widely used because inversion stability and reasonable model constraints are introduced in a framework that fits naturally with least squares algorithms, i.e. the objective function involves a quadratic function of the model. The resulting models, however, tend to have smooth variations that may not always be physically appropriate [*Silva et al.*, 2001; *Bertete-Aguirre et al.*, 2002]. This can be the case when a geologic feature such as a fault or dike has material properties that vary over relatively short distances, or where fluid flow occurs along restricted high permeability pathways. Another case where parameters should not be expected to vary smoothly involves the source term for certain potential field problems. Potential field sources can be highly localized, such as

a cavity that produces a gravity anomaly or a pumping well that produces a self-potential signal. Forms of regularization that do not penalize sharp or blocky features should therefore be used in appropriate circumstances.

In this study, we investigate the use of two alternative types of regularization that provide inversion stability, but do not penalize sharp contrasts in the model. *Last and Kubik* [1983] present a compactness criteria for gravity inversion that seeks to minimize the volume occupied by the causative body. This concept is further developed by *Portniaguine and Zhdanov* [1999] who use the term minimum support (MS) to describe the regularization functional. *Ajo-Franklin et al.* [2006, this report] show an example of compactness constraints for seismic traveltime tomography. The second regularization method we study is total variation (TV), which is essentially a measure of the L_1 norm of the gradient of the model. Total variation therefore requires that the variation of the model is bounded, but does not penalize sharp (or smooth) model gradients. TV has been applied in various forms to geophysical inverse problems [*Claerbout and Muir*, 1973; *Portniaguine and Zhdanov*, 1999; *Yu and Dougherty*, 2000; *Bertete-Aguirre et al.*, 2002], and has also been developed for noise suppression in image processing [*Rudin et al.*, 1992; *Acar and Vogel*, 1994].

Compactness and total variation constraints involve nonlinear functions of the model. Therefore, the objective function is no longer quadratic, and iterative methods must be used to solve the non-linear inverse problem. Iteratively reweighted least squares (IRLS) algorithms have been used effectively to compute solutions using a general L_p norm, typically for $1 \le p \le 2$ [*Scales et al.*, 1988; *Bube and Langan*, 1997; *Farquharson and Oldenburg*, 1998]. The IRLS methodology is readily adapted to both the compactness and total variation constraints that are investigated in this study.

2 Overview of Methods

The general inverse problem that we consider involves the minimization of an objective function (Φ) that is a combined measure of data misfit (ϕ_d) plus one or more stabilizing functionals (ϕ_m, ϕ_x), given in equation (1).

$$\Phi(\mathbf{m}) = \phi_d + \lambda_m^2 \phi_m + \lambda_x^2 \phi_x = \left\| \mathbf{G}\mathbf{m} - \mathbf{d} \right\|_2^2 + \lambda_m^2 \left\| \mathbf{W}_m \left(\mathbf{m} - \mathbf{m}_0 \right) \right\|_2^2 + \lambda_x^2 \left\| \mathbf{W}_x \mathbf{m} \right\|_2^2 \tag{1}$$

$\mathbf{G}$ is a linear operator that maps the model ($\mathbf{m}$) to a data vector ($\mathbf{d}$). In practice, this first term of the objective function is often scaled by a data covariance matrix ($\mathbf{W}_d$), though this has been omitted here. The second term of the objective function is a weighted measure of model length with respect to a prior model ($\mathbf{m}_0$). $\mathbf{W}_m$ is often the identity matrix, but this operator can also be used to incorporate sensitivity information or depth weighting [*Li and Oldenburg*, 1996]. When $\mathbf{W}_m = \mathbf{I}$ and $\mathbf{m}_0 = 0$, $\mathbf{m}$ is biased towards a minimum length solution. The third term of the objective function involves a discrete 1st or 2nd order differential operator ($\mathbf{W}_x$) applied to the model, which provides inversion stability while biasing the solution towards flat or smooth models. Additionally, $\mathbf{W}_x$ can be split into multiple terms; for example, the gradient operator can be split into horizontal and vertical components with different values of λ to promote layered structures. λ_x and λ_m are trade-off parameters that control the relative contributions of the terms in the objective function.

The choice of a linear operator for $\mathbf{W}_m$ and $\mathbf{W}_x$ is convenient when a least-squares solution is sought because the constraints are quadratic functions of $\mathbf{m}$, and have well-behaved minima. The standard least-squares solution that minimizes Φ is found by solving for the value of $\mathbf{m}$ that satisfies $\partial\Phi(\mathbf{m})/\partial\mathbf{m} = \mathbf{0}$

$$\left(\mathbf{G}^T\mathbf{G} + \lambda_m^2 \mathbf{W}_m^T \mathbf{W}_m + \lambda_x^2 \mathbf{W}_x^T \mathbf{W}_x \right) \mathbf{m} = \mathbf{G}^T\mathbf{d} + \lambda_m^2 \mathbf{W}_m^T \mathbf{W}_m \mathbf{m}_0 \,. \tag{2}$$

Besides providing some constraint on the properties of the model, $\mathbf{W}_m$ and $\mathbf{W}_x$ introduce stability for the inverse problem since $\mathbf{G}^T\mathbf{G}$ is often ill-conditioned. For linear problems, $\mathbf{m}$ is recovered in a single inversion step.

Models that satisfy the constraints given in equation (1) tend to be smooth because of the choice of regularization operators described above. In cases where model properties are known to have certain spatial characteristics, this information should be incorporated into the inverse problem. Several examples where properties may not vary smoothly include imaging geologic targets such as faults, dikes, salt diapers, or cavities that have properties which are relatively localized within the area of interest. Time-lapse imaging of fluid injection or removal is another case where the change in geophysical response may be highly localized within zones of relatively high permeability, and could benefit from non-smooth regularization.

2.1 Compactness

One alternative regularization method, developed within the framework of gravity inversion [*Last and Kubik*, 1983], seeks to minimize the area of the causative body. This provides a means for introducing inversion stability while maintaining desirable geologic characteristics. Their formulation for the area, which can easily be extended to volume in three dimensions, is given in equation (3).

$$area = a_e \lim_{\beta \to 0} \sum_{i=1}^{M} \frac{m_i^2}{\left(m_i^2 + \beta^2\right)} . \tag{3}$$

Here, a_e represents the area of an individual model block or element, which is assumed constant in this case. β is a small number that is introduced to provide stability as $m_i \rightarrow 0$. Methods for the selection of β are discussed later. In the limit of $\beta \rightarrow 0$, terms in equation (3) evaluate to 1 for any value of $m_i \neq 0$, and they become 0 for $m_i = 0$. This metric approximates the area of the anomalous region, and is essentially the same as the "minimum support" functional discussed by *Portniaguine and Zhdanov* [1999].

To incorporate the compactness constraint, we minimize a new objective function:

$$\Phi(\mathbf{m}) = \phi_d + \lambda_c^2 \phi_c = \left\| \mathbf{Gm - d} \right\|_2^2 + \lambda_c^2 \sum_{i=1}^{M} \frac{m_i^2}{\left(m_i^2 + \beta^2\right)} . \tag{4}$$

The second term in equation (4) involves a non-linear function of the model. We therefore use an iterative least squares approach to solve for **m** by linearizing this function. This is accomplished with a new diagonal weighting operator, $\mathbf{W}_c$,, which is a function of a previous estimate of the model, $\mathbf{m_{(k-1)}}$.

$$\mathbf{W}_{c_{ii}}^k = \left(m_{(k-1)_i}^2 + \beta^2\right)^{-1/2} \tag{5}$$

The least squares solution for the new model estimate $\mathbf{m_{(k+1)}}$ then becomes

$$\left(\mathbf{G}^T\mathbf{G} + \lambda_c^2 \mathbf{W}_c^{k^T} \mathbf{W}_c^k\right)\mathbf{m}_{(k+1)} = \mathbf{G}^T\mathbf{d} . \tag{6}$$

A common approach is to use one of the conventional linear regularization operators discussed at the beginning of section 2 for the first iteration. This smooth model is then used to generate a new weighting matrix, which is in turn used to solve for a new **m**. The IRLS process is continued until there is little difference between successive models, or some other convergence criteria is met.

Figure 1 shows a comparison between the model regularization terms ϕ_m and ϕ_c for a simple linear operator ($\mathbf{W} = \mathbf{W}_m = \mathbf{I}$) and the compactness operator ($\mathbf{W} = \mathbf{W}_c$). This figure illustrates some important differences between these constraints. In the former case, large values of **m** are increasingly penalized because the function is parabolic, which results in a minimum length model. For the compactness constraint, the function quickly asymptotes to 1; therefore, large values of **m** are not penalized more than small to intermediate values. ϕ_c is minimized by reducing as many model parameters to zero as possible while still satisfying the data misfit term. As β becomes smaller, this curve becomes sharper, effectively setting a threshold for the 'on-off' value of **m**.

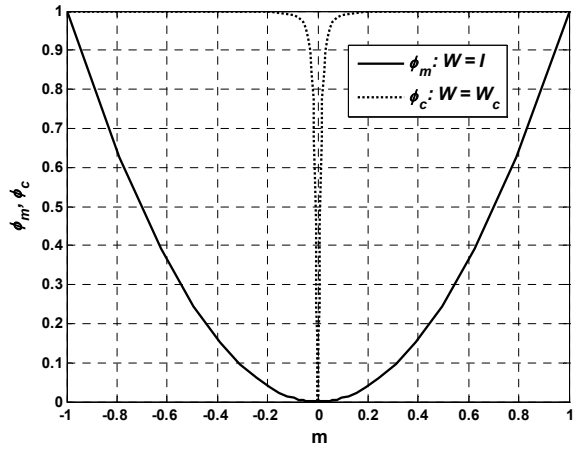

Figure 1. Comparison of the model regularization terms ϕ_m and ϕ_c. The solid line shows the traditional quadratic function ϕ_m typical of a linear operator applied to the model. The dashed line shows ϕ_c for the compactness operator with $\beta^2 = 1e^{-4}$.

2.2 Total Variation

A second method of regularization that provides inversion stability while allowing for non-smooth models is total variation. The TV functional is a measure of the variation of the model, and is essentially the L_1 norm of the gradient of the model [e.g. *Acar and Vogel*, 1994; *Bertete-Aguirre et al.*, 2002], as stated in equation (7). Minimiza-

tion of the total variation seeks to generate "blocky" images that are piecewise constant over one or more regions [*Claerbout and Muir*, 1973; *Dobson and Santosa*, 1996]. Both L_1 and L_2 norms of the gradient penalize oscillations in the model due to noisy data. Sharp discontinuities are better preserved under the L_1 norm, however, because the total variation measures the sum of gradients rather than their squared values.

$$\phi_{TV}(\mathbf{m}) = \int_{\Omega} |\nabla \mathbf{m}| \, d\mathbf{r} \tag{7}$$

Because equation (7) is non-differentiable when $\nabla\mathbf{m} = 0$, the total variation functional is often approximated using equation (8) [e.g. *Farquharson and Oldenburg*, 1998; *Bertete-Aguirre et al.*, 2002].

$$\phi_{TV}(\mathbf{m}) = \left(|\nabla \mathbf{m}|^2 + \beta^2 \right)^{1/2} \tag{8}$$

This is a specific case of the generalized measures of data misfit and model structure discussed by *Farquharson and Oldenburg* [1998]. The gradient operator is replaced with $\mathbf{W}_x$, the discrete linear difference operator discussed earlier. Differentiating with respect to $\mathbf{m}$ then leads to

$$\frac{\partial \phi_{TV}(\mathbf{m})}{\partial \mathbf{m}} = \mathbf{W}_x^T \mathbf{R}_x \mathbf{W}_x \mathbf{m} \tag{9}$$

where,

$$\mathbf{R}_{x_{ii}} = \frac{1}{\left(\left(\mathbf{W}_x \mathbf{m} \right)_i^2 + \beta^2 \right)^{1/2}} . \tag{10}$$

$\mathbf{R}_x$ is a diagonal matrix with an entry for differences between model parameters in all directions. β plays a similar role to the compactness example, in this case providing stability when the model gradient is near zero. Minimization of the full objective function, $\Phi(\mathbf{m}) = \phi_d + \lambda_{TV}^2 \phi_{TV}$, results in the familiar system of equations for $\mathbf{m}$ given in equation (11).

$$\left(\mathbf{G}^T \mathbf{G} + \lambda_{TV}^2 \mathbf{W}_x^T \mathbf{R}_x^k \mathbf{W}_x \right) \mathbf{m}_{(k+1)} = \mathbf{G}^T \mathbf{d} \tag{11}$$

An iterative approach must again be used because the total variation constraint involves a non-linear function of the model. As with the compactness example, the first estimate for $\mathbf{m}$ typically comes from a conventional linear smoothness constraint. This model is then used to compute a new diagonal weighting matrix $\mathbf{R}_x^k$ and, subsequently, a new model estimate, $\mathbf{m}_{(k+1)}$.

2.3 Choosing β

β is an important parameter for both compactness and total variation constraints. Its main purpose is to avoid singularities in equation (4), and to provide differentiability in equation (8). In general, we are interested in the case where $\beta \to 0$, though there are practical limitations due to noisy data and limited sensitivities. For instance, the dashed curve in Figure 1 shows the compactness term of the objective function in equation (4) as a function of β. As β becomes smaller, the notch near zero becomes sharper such that model parameter values must be reduced below this level in order to reduce the compactness term in the objective function. For a certain level of noise, however, it will not be possible to reduce parameter values beyond a certain threshold and still fit the data. Conversely, $\mathbf{W}c \to \beta^{-1}$ in equation (5) as β becomes large, which acts like a weighted minimum length constraint on the model.

Similar considerations are made for β in the total variation case; a value is chosen such that it provides a balance between the desired L_1 norm approximation and inversion stability. A trade-off curve method is generally used to select β by computing ϕ_c or ϕ_{TV} for the current model estimate over a range of values for β [*Farquharson and Oldenburg*, 1998; *Zhdanov and Tolstaya*, 2004]. This concept is similar to the L-curve methods used to select the traditional regularization parameter, λ [*Hansen*, 1992]. A simple illustration of this procedure is shown in Figure 2, where the 'optimal' value is chosen at the point of maximum curvature on a log-log plot. This ensures that inversion stability is maintained while the value of the objective function does not deviate strongly from its value when $\beta = 0$.

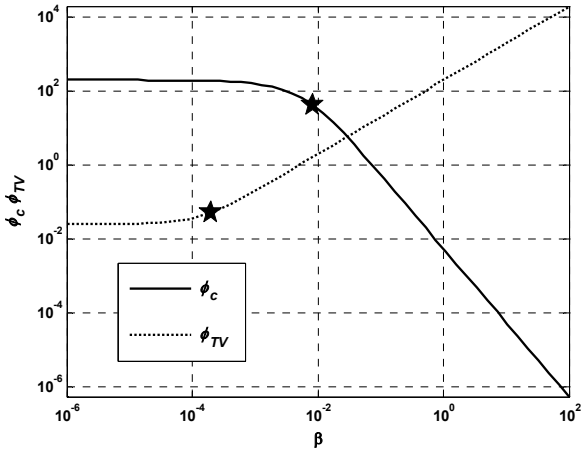

Figure 2. Trade-off curves that illustrate the selection of β for the compactness and total variation constraints. The objective function for the current model is calculated for multiple values of β, and a value is chosen near the point of maximum curvature (indicated by stars). This value of β is then used to compute a new model estimate.

3 Synthetic Potential-Field Examples

3.1 Self-Potential Source Inversion Background

We illustrate the effect of the various model constraints discussed so far using a synthetic 2D self-potential source inversion example. Here, self-potential data refer to electrical potentials measured on the earth surface or in a borehole. These potentials, φ [V], arise from the coupling of a source term, $\mathbf{s}$ [A·m^{-3}], with the earth resistivity structure, $1/\boldsymbol{\sigma}$ [Ω·m], as defined in equation (12).

$$\nabla \cdot \boldsymbol{\sigma} \nabla \varphi = \mathbf{s} \tag{12}$$

Details on the generation of self potential sources can be found in many articles [e.g. *Sill*, 1983; *Morgan et al.*, 1989; *Revil et al.*, 1999], but will not be discussed in this paper. Equation (12) is an elliptic PDE that is relevant to other potential-field problems such as gravity and magnetics.

To solve the self-potential problem, equation (12) is discretized using the transmission network analogy [e.g. *Zhang et al.*, 1995; *Shi*, 1998], resulting in the linear system of equations given in (13).

$$\mathbf{K}\varphi = \mathbf{s} \tag{13}$$

K is a sparse, positive definite symmetric operator that incorporates the model geometry, resistivity information, and boundary conditions. Incorrect assumptions about the resistivity structure are an important source of error, but we use a homogeneous resistivity structure for the following examples in order to highlight the effects of the different model constraints covered in this paper.

Given a source term, **s**, the calculation of potentials throughout the model is well-posed due to the properties of **K**. The self-potential source inversion problem of interest, however, is ill-posed. Our goal is to recover the source vector from an incomplete set of electrical potential measurements φ_d, which is stated in equation (14).

$$\varphi_d = \mathbf{P}\varphi = \mathbf{P}\mathbf{K}^{-1}\mathbf{s} = \mathbf{G}\mathbf{s} \tag{14}$$

P is a sparse 'picker' matrix with a single 1 on each row that selects the locations where data are measured. The operator **G** is therefore a subset of the rows of the full matrix $\mathbf{K}^{-1}$, and can be computed effectively using reciprocity [*Minsley et al.*, 2006]. Equation (14) is therefore used to define the data misfit term ϕ_d in the objective function, where

$$\phi_d = \left\| \mathbf{G}\mathbf{s} - \varphi_d \right\|_2^2 \tag{15}$$

3.2 Synthetic Model and Sensitivities

A 2D source model is shown in Figure 3, along with synthetic noise-free data simulated at measurement locations on the earth surface. The model is 60 x 20 (M = 1,200) and N = 58 measurements are shown. The negative point source is given a value of -3mA, and each pixel in the dipping source is +1.5mA. The resistivity values are assigned to 1 Ω·m throughout the model for simplicity.

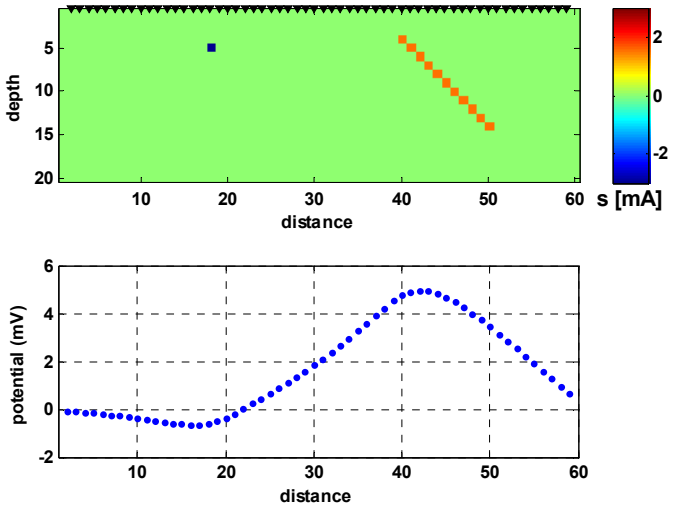

Figure 3. True model ($\mathbf{s_{true}}$) used for synthetic examples with 1,200 parameters (top). There is a negative point source towards the left, and a positive dipping source on the right hand side. Data locations are simulated along the earth surface, indicated by ▼. The bottom panel shows the synthetic noise-free data, φ_d, at the measurement locations.

Due to the decrease in sensitivity with distance from the measurement locations, it is common in potential-field inversions to perform some sort of sensitivity scaling or depth weighting [*Li and Oldenburg*, 1996]. The sensitivity information can be incorporated with any of the regularization operators discussed already. For this problem, we define the 'cumulative sensitivity' using equation (16)

$$\mathbf{W}_{s_{jj}} = \sqrt{\sum_{i=1}^{N} \mathbf{G}_{ij}^2} \,. \tag{16}$$

$\mathbf{W}_s$ is a diagonal operator whose entries are derived from the sum of the squared elements in each column of $\mathbf{G}$. This represents the 'cumulative sensitivity' of each model parameter to all of the measurement locations. Figure 4 shows the elements of $\mathbf{W}_s$ for the model defined above.

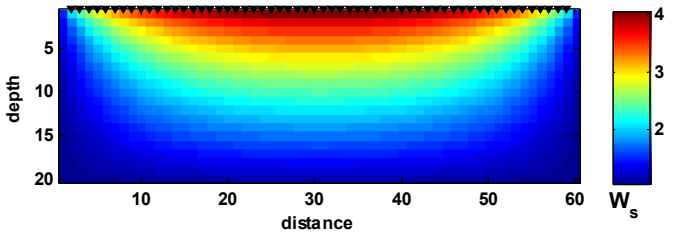

Figure 4. Cumulative sensitivities for the model shown in Figure 3.

3.3 Inversion Results with Traditional Constraints

Figure 5 shows source inversion results using the traditional linear constraints discussed in the beginning of section 2. The top panel shows the solution with $\mathbf{W}_m = \mathbf{I}$ for the constraint, the middle panel shows the result using a differencing operator $\mathbf{W}x = \nabla$ for the constraint, and the bottom panel shows the result when $\mathbf{W}x = \nabla^2$ is the constraint. In all three cases, the sensitivity operator $\mathbf{W}_s$ is included in order to provide solutions that are not pulled strongly towards the measurement locations. The white asterisks indicate the true source locations, and the regularization parameter, λ, is set to 0.1 for all examples. The 1st and 2nd order differential operator smoothing results are very similar (middle and bottom panel), though the 2nd order result provides slightly larger amplitudes.

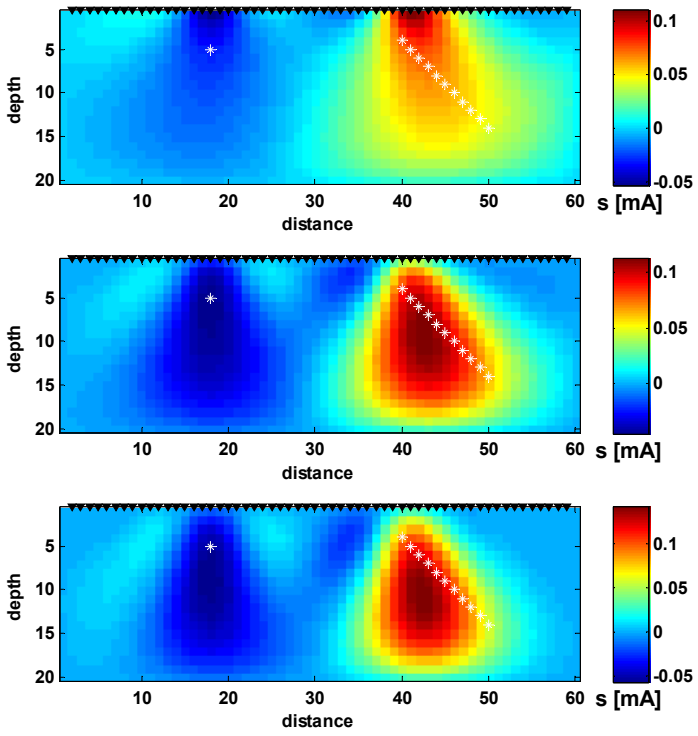

Figure 5. Inversion results using the data shown in Figure 3 using traditional linear constraints: minimum length $\mathbf{W}_m$ (top), discrete gradient $\mathbf{W}x = \nabla$ (middle), discrete laplacian $\mathbf{W}x = \nabla^2$ (bottom). White asterisks indicate the true source locations.

We also investigate the effects of noisy data on the inversion using the 2nd order differential operator as a smoothness constraint. 10% Gaussian noise is added to the data, and the resulting source model is shown in Figure 6. There are several near-surface artifacts in the model due to oscillations in the data, though the model prediction does a good job of depicting the main trends without over-fitting the data, as seen in the bottom panel of this figure. The main positive and negative features related to the true sources are slightly distorted with respect to the noise-free example, though the amplitudes remain nearly equal.

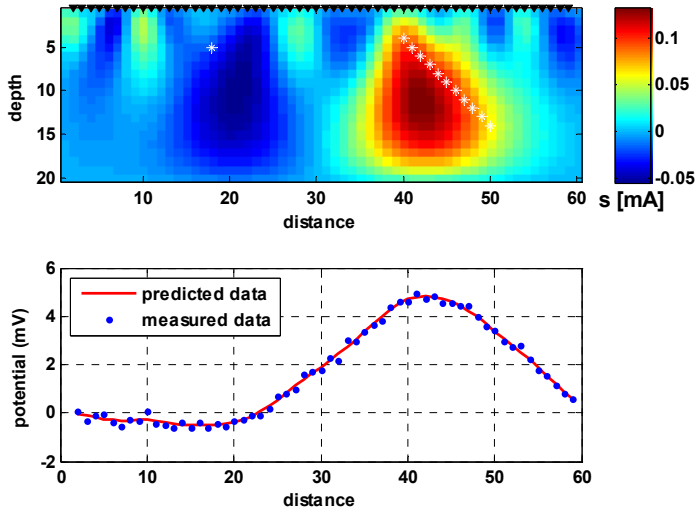

Figure 6. Source inversion using the same 2nd order smoothing operator as the bottom panel in Figure 5, but 10% Gaussian noise is added to the data (top). Noisy input data and the data predicted by this model are also shown (bottom)

3.4 Inversion Results with the Compactness Constraint

Next, we examine the effects of implementing the non-linear compactness constraint discussed in section 2.1. One benefit of this approach is that an ensemble of increasingly compact models are generated, starting with one of the smoothed models using a linear constraint. Because each iteration produces nearly the same data fit, the 'correct' model must be chosen based on some prior knowledge about the source structure.

Starting with the 2nd order smoothed model in the bottom of Figure 5, a new weighting operator is computed according to equation (5), which is used to find a more compact model using equation (6). This process is repeated for several IRLS iterations, with a new β at each step based on the trade-off curve method described earlier. Again, the regularization parameter λ_c is fixed at 0.1. Figure 7 illustrates the re-weighted regularization operators (panels B, D, and F) and resulting source models (panels A, C, and E) for iterations 3, 5, and 7. It is useful to think of the regularization operator as a spatially-varying damping matrix, where small weights (i.e. low damping) are assigned to areas where the model amplitudes are large. Where model estimates are small, the weights become large so that these parameters are forced towards zero, as long as the data allow it.

As expected, the sources become more focused as the iterations proceed. Additionally, the source amplitudes increase with increasing compactness in order to fit the data. Potential-field inversions are often plagued by the problem of non-uniqueness that allows for either shallow/diffuse sources or deep/compact sources. The compactness constraint therefore naturally incorporates sources at depth as long as the data misfit term is satisfied.

In panel E, it appears that the compactness constraint has been carried out too far as the positive dipping anomaly appears broken. While this may partially be the case due to the limited surface data available, it is useful to also look at the regularization operator in panel F. The constraints over the entire length of the dipping source are very small, indicating that the source amplitudes are still greater than β. The fact that some values along the dipping anomaly are larger than others can be attributed to the fact that the problem is still non-unique, and the limited surface data are not adequate to fully describe the source.

The case of noisy data is also considered for the compactness example, which is illustrated in Figure 8. Noise in the data clearly impacts the ability to reconstruct the true source image, though the general locations of the sources are still captured. Surface artifacts that affect the solution found with the linear regularization operator are damped out during the compactness iterations, however. Subtle features in the data due to a dipping or distributed source are masked by the noise, limiting the extent to which these features can be imaged. As the level of noise in the data increases, one should limit the compactness of the recovered model. This can be partially explained by the traditional resolution matrix, $\mathbf{R}$, where $\mathbf{m} = \mathbf{R}\mathbf{m}_{true}$. For the compactness case, $\mathbf{R}$ is a function of a prior model estimate, and is therefore data-dependent. Thus, as the data quality becomes poorer, we should expect results with correspondingly low resolution.

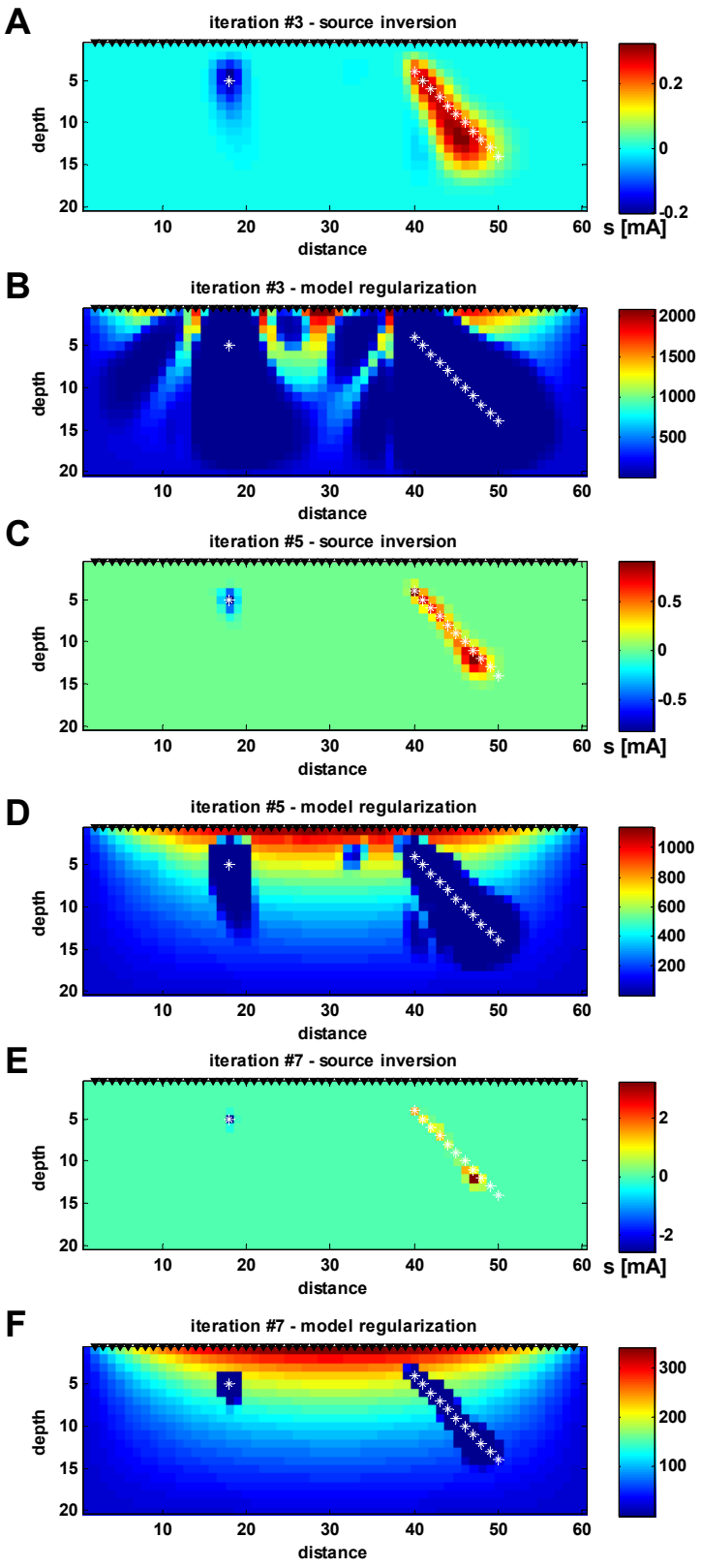

Figure 7. Source inversion results and re-weighting regularization operators for compactness IRLS iterations 3 (A-B), 5 (C-D), and 7 (E-F).

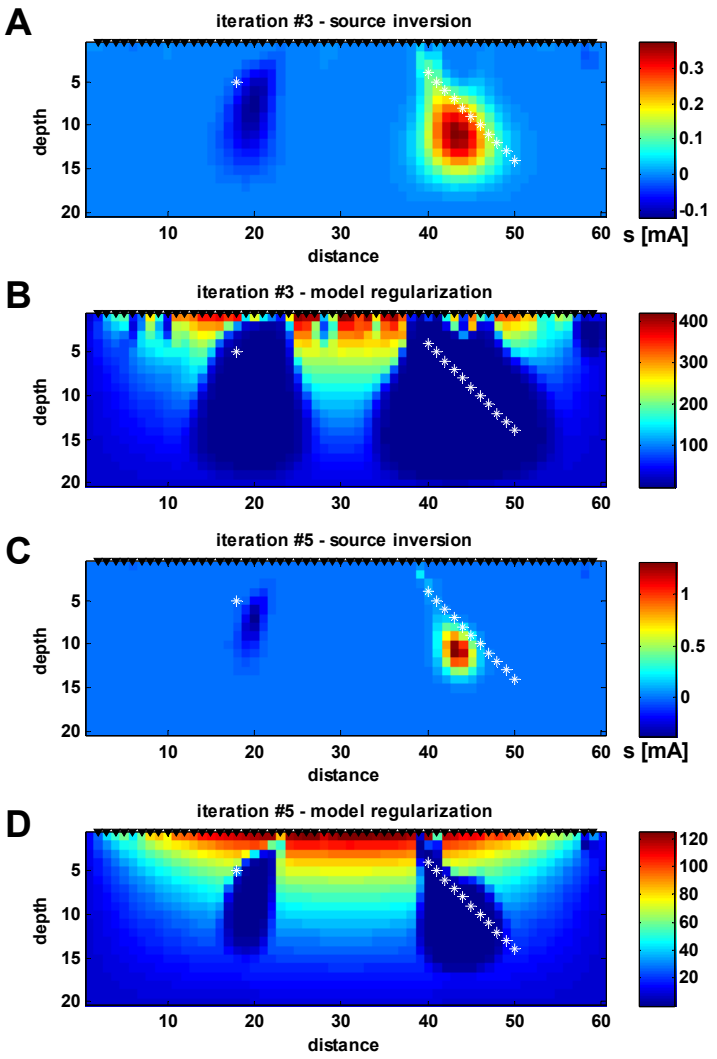

Figure 8. Source inversion results and re-weighting regularization operators for compactness IRLS iterations 3 (A-B) and 5 (C-D) using noisy data

3.5 Inversion Results with the Total Variation Constraint

The final synthetic example uses the non-linear total variation constraint described in section 2.2 for the source inversion problem. Results for the noise-free case are shown in Figure 9, again with $\lambda_{TV} = 0.1$, for iterations 3 (A-B), 5 (C-D), and 7 (E-F). The starting model for the total variation example is the smooth model from the last panel of Figure 5, which used the linear 2nd order regularization operator. The source inversion results for is example (A, C, and E in Figure 9) show the 'blocky' behavior that we expect from the total variation regularization. Changes in the model between iterations are less dramatic than the compactness example, however. The model regularization operators shown in panels B, D, and F are also more complicated than in the compactness case.

In the process of minimizing the total variation functional, the model becomes more focused, though the solution is still somewhat smoothed. While this method helps to sharpen edges in the model and delineate the source regions, there is no explicit constraint that the model should be come increasingly compact. In fact, the total variation measure of the true source model is greater than any of the source results shown in Figure 9. Thus, the total variation constraint has not failed (the algorithm has successfully minimized the objective function); it is simply not the best measure of the true model.

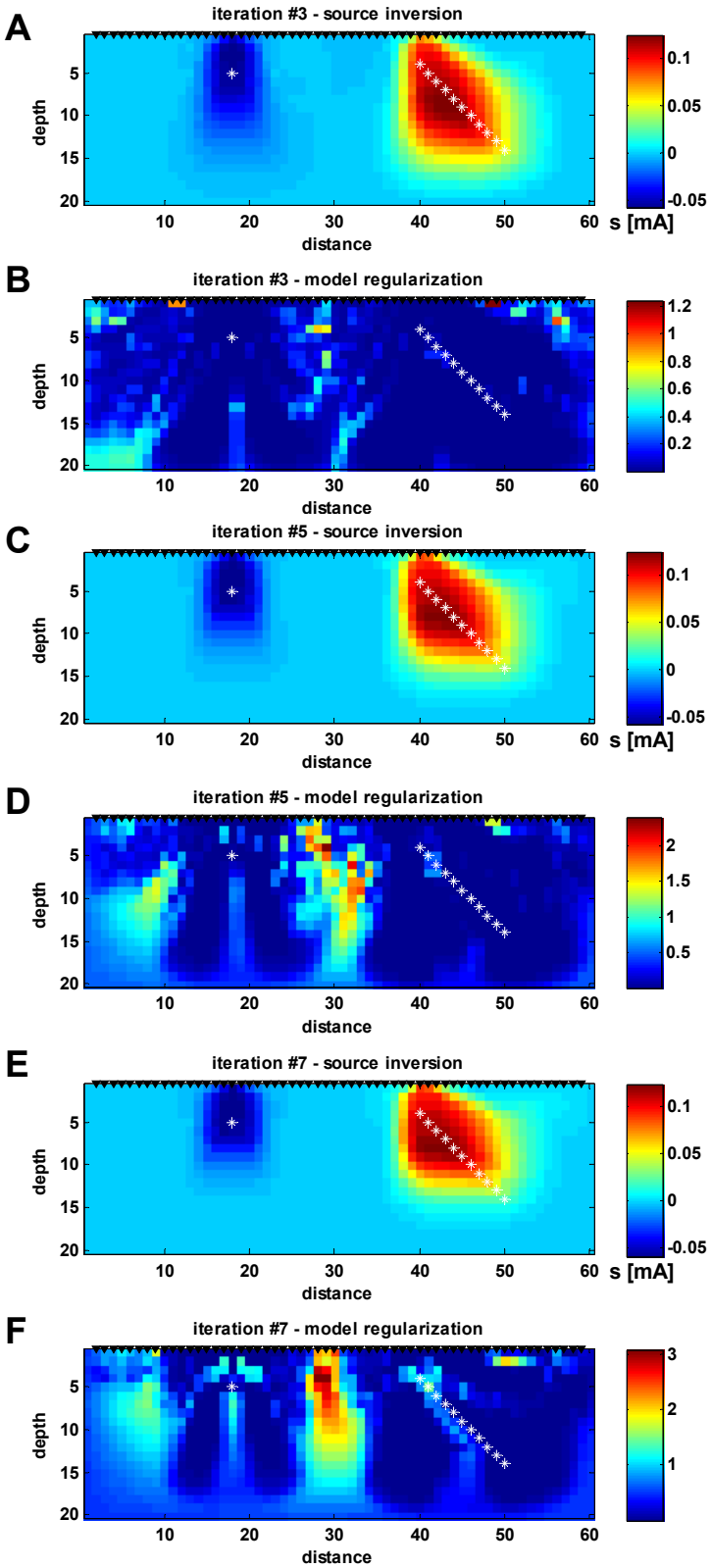

Figure 9. Source inversion results and re-weighting regularization operators for total variation IRLS iterations 3 (A-B), 5 (C-D), and 7 (E-F).

4 Field Data Example using the Compactness Constraint

Our final example uses the compactness method on a field self-potential dataset collected in the vicinity of a pumping well. The data were originally published by *Bogoslovsky and Ogilvy* [1973], and have been more recently analyzed by several other authors [*Darnet et al.*, 2003; *Revil et al.*, 2003; *Minsley et al.*, 2006]. One primary source of self-potential signals can be attributed to locations where there is a divergence of fluid flow [*Sill*, 1983]. Thus, this well-pumping dataset provides a good example of a case where we should expect a fairly isolated self-potential source at the screened portion of the well. The code used to process this dataset operates on the same principles discussed for the synthetic example, but uses a 3D geometry. It is important to account for the 3D flow of electrical currents when modeling real field data in the earth.

Figure 10 shows the self-potential profile (top) collected over the pumping well (labeled K-1) as well as the water table elevations interpolated from piezometers in several monitoring wells (bottom). The broad positive anomaly is fairly symmetric about the well position, and there are two sharp negative anomalies that correspond to infiltration from the surface drainage ditches located at approximately -70m and +110m. As expected with field data, there is some noise that corrupts the signal.

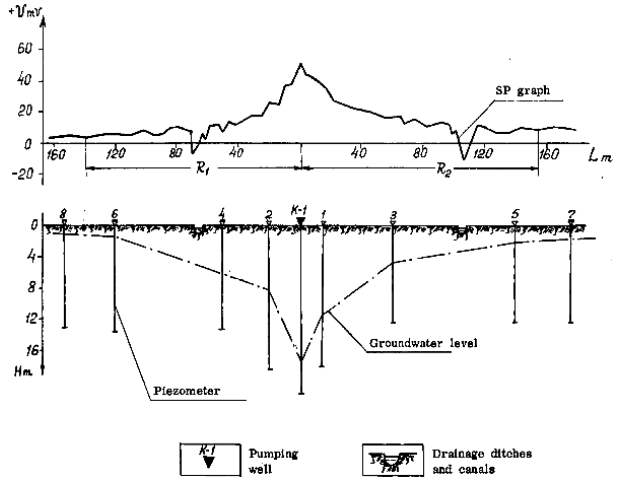

Figure 10. Self-potential profile (top) in the vicinity of a pumping well (K-1, bottom). The water table elevation is estimated in the bottom part of the figure from piezometers in monitoring wells. Note the influence of infiltration from the surface drainage ditches near -70 and +110m on the self-potential signal. 85 SP measurements are discretized from the original figure [*Bogoslovsky and Ogilvy*, 1973].

For the self-potential inversion, we have discretized the data at 85 locations with 4m spacing. A 3D model is generated with dimensions (101 x 21 x 33) nodes (M = 69993), with 4m node spacing in the x-y direction and 1m in depth, except for the larger boundary nodes. A small y-dimension can be used because, while the problem is 3D, the data lie entirely on a 2D profile. The result of this geometry is that sources can only be properly collapsed onto the vertical plane through the data, which is suitable for this particular problem. Details about the resistivity structure are unknown, but we use a 2D resistivity approximates the unsaturated drawdown cone. This model consists of a 1m surface layer of 150Ω·m over a 40Ω·m half-space, in which we add a radially symmetric region of 85Ω·m in the drawdown region estimated from the bottom of Figure 10.

Noise in the data that has a high spatial frequency (uncorrelated noise) tends to produce unwanted large amplitude artifacts in the source model near the surface measurements. To address this, we include a strong smoothness constraint ($\min \left\| \nabla^2 \mathbf{s} \right\|^2$) that is relaxed as the iterative re-weighting iterations proceed. The smoothness constraint ensures that the gross model structure is estimated and the noise artifacts are damped out for the first iteration. The minimum support operator is therefore not biased towards focusing the surface artifacts, and solutions at depth can be found. As the sources move away from the measurement locations, the smoothness constraint is no longer needed because the near-surface artifacts do not improve the data misfit.

Six different source estimates are shown in Figure 11, starting with the smoothed model at the top (iteration 1), then successively more compact model estimates (iterations 4, 7, 10, and 13). The groundwater elevations, pumping well, and drainage ditches are superimposed on each image. In all three cases there is a large positive source at depth in the vicinity of the screened portion of the well where fluid is removed. The two drainage ditches

where there is infiltration into the subsurface show up nicely as near-surface sources with negative polarity, and smaller amplitude than the pumping source.

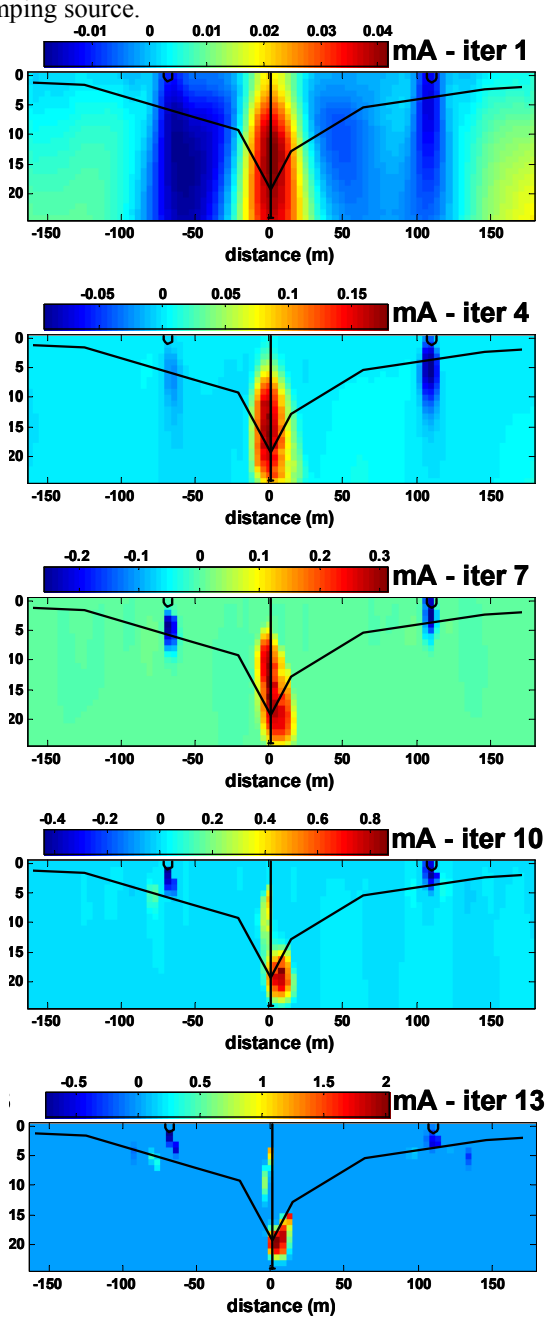

Figure 11. Source estimates for the field data example, starting with a smooth model (top) using a traditional linear 2nd order constraint. Increasing compactness, observed from top to bottom for each example, is due to the iterative re-weighting. A smoothness constraint is enforced during the early iterations to remove the influence of noisy data, and is subsequently relaxed as the compact source solution becomes more stable. The location of the water table, pumping well, and drainage ditches are superimposed on the source images.

Figure 12 shows the data fit for three of the minimum support iterations. The effect of the smoothness constraint on the early iterations is evident in this figure; the first model estimate captures only the general features of the data, but provides a useful approximation for the next iterative weighting term.

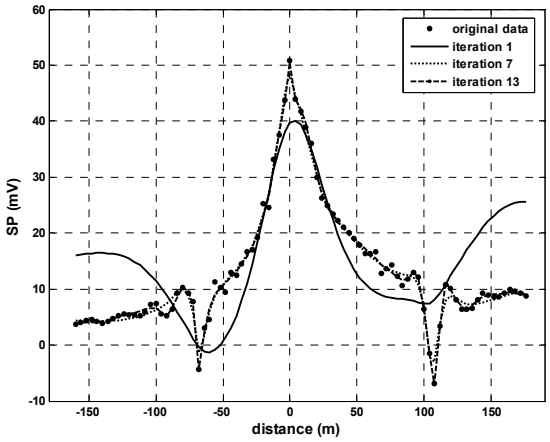

Figure 12. Data fit for three iterations of the compact source solution. Note the rough fit for the first iteration, which has a strong smoothness constraint to avoid near surface artifacts due to the noisy data. This constraint is relaxed at later iterations, which is evident by the improved data fit.

Without knowing the details about the screened portion of the pumping well, pumping rate, or true resistivity structure, it is difficult to calibrate these results. We expect, however, that there should be a relatively compact source at the portion of the well where fluid is removed. The deeper source solution for iterations 10-13 best represents pumping somewhere between the groundwater level of 17m at the well and well depth of ~22m.

5 Conclusions

We have presented two alternative non-linear model regularization strategies, compactness and total variation, which attempt to incorporate prior information about model structure when traditional smoothness constraints do not capture the expected model behavior. Because both methods are solved iteratively, an ensemble of solutions is generated as the objective function is minimized. It is often instructive to view several different models that fit the data equally well in order to determine which one best meets the prior knowledge about model structure.

For potential-field problems where sources are expected to be somewhat localized, the compactness constraint provides a natural tendency for solutions at depth, which helps to overcome some of the non-uniqueness in the problem. This effect is clearly illustrated using the synthetic examples. Total variation, on the other hand, does not explicitly enforce compactness, but produces images with sharper edges, which helps to delineate source regions. One interesting study might involve a hybrid compactness-total variation constraint that could produce localized sources that are also required to be flat. This could be useful in gravity inversion, for example, where an intrusion of constant density is sought.

Limitations due to noisy data are also addressed in the synthetic examples. Because the regularization operators for both compactness and total variation are dependent on prior model estimates, the resolution becomes data-dependant. For this reason, we should expect decreased resolution as the level of noise increases in the data. Several options to address noise include: increasing β to produce more of a damping effect, adding a small amount of a traditional smoothness constraint to the inversion, and starting with an over-damped initial model to reduce the influence from high frequency oscillations.

Application of the compactness constraint to the self-potential field data example is successfully able to locate isolated sources. Future work will be directed towards 1) adding total variation constraints to the 3D source inversion, 2) determining optimal methods to handle noisy data, and 3) using prior information to determine appropriate convergence criteria.

6 Acknowledgements

We would like to thank the Earth Resources Laboratory Founding Members and the Kuwait-MIT Center for Natural Resources and the Environment for providing funding that supported this work.

References

Acar, R., and C.R. Vogel (1994), Analysis of Bounded Variation Penalty Methods for Ill-Posed Problems, *Inverse Probl.*, *10* (6), 1217-1229.

Ajo-Franklin, J.B., B.J. Minsley, and T.M. Daley (2006), Applying compactness constraints to seismic traveltime tomography, Earth Resources Laboratory Industry Consortium Meeting, Cambridge, Massachusetts.

Bertete-Aguirre, H., E. Cherkaev, and M. Oristaglio (2002), Non-smooth gravity problem with total variation penalization functional, *Geophys. J. Int.*, *149* (2), 499-507.

Bogoslovsky, V.A., and A.A. Ogilvy (1973), Deformations of natural electric fields near drainage structures, *Geophys. Prospect.*, *21*, 716-723.

Bube, K.P., and R.T. Langan (1997), Hybrid l^1/l^2 minimization with applications to tomography, *Geophysics*, *62* (4), 1183-1195.

Claerbout, J.F., and F. Muir (1973), Robust Modeling with Erratic Data, *Geophysics*, *38* (5), 826-844.

Darnet, M., G. Marquis, and P. Sailhac (2003), Estimating aquifer hydraulic properties from the inversion of surface Streaming Potential (SP) anomalies, *Geophys. Res. Lett.*, *30* (13), doi:10.1029/2003GL017631.

Dobson, D.C., and F. Santosa (1996), Recovery of blocky images from noisy and blurred data, *Siam J Appl Math*, *56* (4), 1181-1198.

Farquharson, C.G., and D.W. Oldenburg (1998), Non-linear inversion using general measures of data misfit and model structure, *Geophys. J. Int.*, *134* (1), 213-227.

Hansen, P.C. (1992), Analysis of Discrete Ill-Posed Problems by Means of the L-Curve, *Siam Rev*, *34* (4), 561-580.

Last, B.J., and K. Kubik (1983), Compact gravity inversion, *Geophysics*, *48* (6), 713-721.

Li, Y., and D.W. Oldenburg (1996), 3-D inversion of magnetic data, *Geophysics*, *61* (2), 394-408.

Li, Y.G., and D.W. Oldenburg (2000), Incorporating geological dip in formation into geophysical inversions, *Geophysics*, *65* (1), 148-157.

Minsley, B., J. Sogade, and F.D. Morgan (2006), 3D source inversion of self-potential data, *submitted to Journal of Geophysical Research 01/06, in revision*.

Morgan, F.D., E.R. Williams, and T.R. Madden (1989), Streaming Potential Properties of Westerly Granite with Applications, *J. Geophys. Res.*, *94* (B9), 12449-12461.

Portniaguine, O., and M.S. Zhdanov (1999), Focusing geophysical inversion images, *Geophysics*, *64* (3), 874-887.

Revil, A., V. Naudet, J. Nouzaret, and M. Pessel (2003), Principles of electrography applied to self-potential electrokinetic sources and hydrogeological applications, *Water Resour. Res.*, *39* (5), 1114, doi:10.1029/2001WR000916.

Revil, A., P.A. Pezard, and P.W.J. Glover (1999), Streaming potential in porous media 1. Theory of the zeta potential, *J. Geophys. Res.*, *104* (B9), 20021-20031.

Rudin, L.I., S. Osher, and E. Fatemi (1992), Nonlinear Total Variation Based Noise Removal Algorithms, *Physica D*, *60* (1-4), 259-268.

Scales, J.A., A. Gersztenkorn, and S. Treitel (1988), Fast L_p Solution of Large, Sparse, Linear-Systems - Application to Seismic Travel Time Tomography, *J. Comput. Phys.*, *75* (2), 314-333.

Shi, W. (1998), Advanced modeling and inversion techniques for three-dimensional geoelectrical surveys, Ph.D. thesis, Massachusetts Institute of Technology, Cambridge, MA.

Sill, W.R. (1983), Self-Potential Modeling from Primary Flows, *Geophysics*, *48* (1), 76-86.

Silva, J.B.C., W.E. Medeiros, and V.C.F. Barbosa (2001), Potential-field inversion: Choosing the appropriate technique to solve a geologic problem, *Geophysics*, *66* (2), 511-520.

Tikhonov, A.N., and V.A. Arsenin (1977), *Solutions of ill-posed problems*, 258 pp., Winston & Sons, Washington.

Yu, M.C., and D.E. Dougherty (2000), Modified total variation methods for three-dimensional electrical resistance tomography inverse problems, *Water Resour. Res.*, *36* (7), 1653-1664.

Zhang, J., R.L. Mackie, and T.R. Madden (1995), 3-D Resistivity Forward Modeling and Inversion Using Conjugate Gradients, *Geophysics*, *60* (5), 1313-1325.

Zhdanov, M., and E. Tolstaya (2004), Minimum support nonlinear parametrization in the solution of a 3D magnetotelluric inverse problem, *Inverse Probl.*, *20* (3), 937-952, doi:10.1088/0266-5611/20/3/017.